Paper 01 / 2026 doi: 10.7795/320.202601

JUNGE wissenschaft

Jungforscher*Innen publizieren
online | *peer reviewed* | original

Verlag:
Physikalisch-
Technische
Bundesanstalt
PTB

Cleaning without water

Electrostatic Cleaning of Photovoltaic Modules in Desert Environments

This work develops a sustainable electrostatic cleaning method for solar panels in desert regions, enabling removal of sand without water or harsh chemicals. Analyses show this method effectively restores PV efficiency, reduces power loss, and offers cost savings, especially in manual use, making it an eco-friendly alternative for large-scale solarenergy production.

DER JUNGFORSCHER

© Schweizer Jugend forscht

Nicholas Kessler (*2004)
Kantonsschule Wohlen

Eingang der Arbeit:
30.4.2025
Arbeit angenommen:
8.8.2025

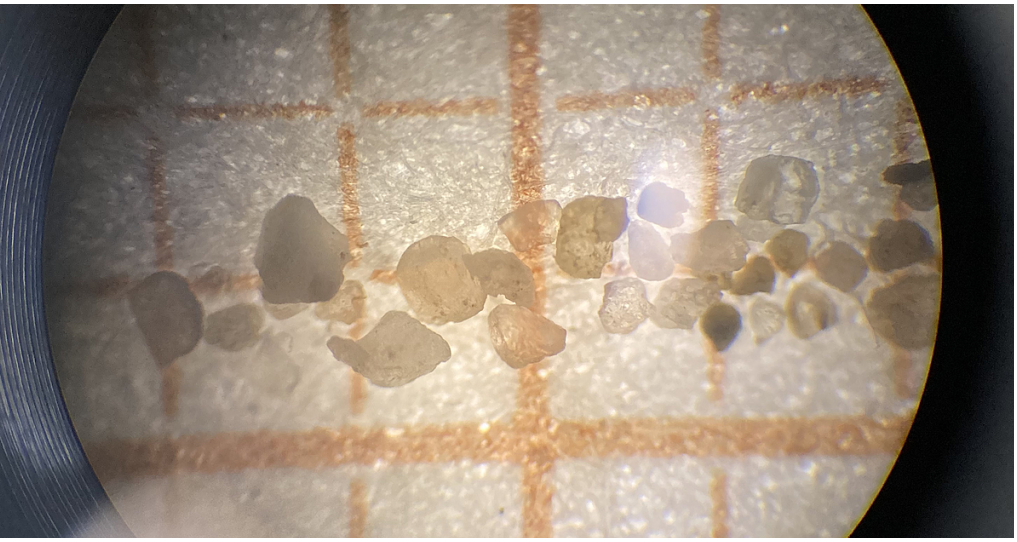

Cleaning without water

Electrostatic Cleaning of Photovoltaic Modules in Desert Environments

1. Introduction

The global demand for renewable energy sources has surged over the past few decades, with sustainable electricity generation accounting for 31 % of the world's total energy production of 2020 [1]. Photovoltaic (PV) energy, in particular, has emerged as a promising alternative to fossil fuels, offering a clean and abundant source of power. However, the widespread use of PV modules has brought to light a significant issue: the accumulation of micro-particles on the surface of PV modules, particularly in arid regions such as deserts.

In such areas, sand deposits on the glass surface of PV modules lead to a major reduction in energy output within months of outdoor exposure [2]. Despite these challenges, desert regions remain lucrative sites for energy generation due to their vast geographical area, abundant sunlight, and favourable weather conditions. Governments and private investors in Europe and China have invested heavily in large-scale energy projects in desert areas, such as the Noor Complex in Morocco and the Tengger Solar Park in China, among others [3].

The problem of sand deposition on PV modules in such areas is generally addressed through costly and environmentally harmful water-based cleaning processes. These methods require frequent cleaning, transportation, and numerous workers [4]. Mechanical cleaning methods also pose challenges, as they often result in scratching the glass surface [5].

This paper presents a novel approach to address the issue of sand contamination on PV modules by utilizing electrostatic forces to remove micro-particles from the surface of PV modules. The proposed electric cleaning method aims to facilitate the waterfree operation of PV modules in subtropical regions. This approach offers a sustainable and cost-effective solution to a pressing environmental and economic problem. This study provides an overview of the challenges associated with PV module maintenance in desert regions. It also presents a novel approach to mitigate the impact of sand deposition on PV module performance.

2. State of the Art

The deposition of airborne particles such as sand and dust on photovoltaic modules, poses a persistent challenge to the efficiency of solar energy. Numerous studies have quantified the adverse impact of surface contamination, reporting energy losses of up to 50 % within months of exposure under severe soiling conditions [2]. Consequently, the mitigation of soiling has become a critical research focus within PV research.

Conventional cleaning methods primarily rely on manual or automated water-based washing [4]. Although operationally simple, such methods are increasingly recognized as unsustainable in desert environments due to high water scarcity, logistical costs, and adverse environmental implications. Mechanical cleaning alternatives, such as brushes or wipers, offer partial relief but risk physical abrasion to the module surface, leading to optical damage [5].

These limitations have motivated the search for waterless, minimally invasive, and energy-efficient cleaning solutions. Recent advances have led to two categories of water-free approaches: passive and active systems. Passive systems rely on material surface modifications that inhibit dust adhesion or promote self-cleaning. Coatings featuring super hydrophobic, oleophobic, or photocatalytic properties have demonstrated potential in laboratory and field conditions. TiO_2-based

doi: 10.7795/320.202601

coatings, in particular, can degrade organic contaminants and enable partial self-cleaning through photocatalytic action and hydrophilicity [6]. However, their long-term performance under persistent sand exposure and extreme thermal cycling remains inconsistent, with degradation and diminished transparency frequently reported. Furthermore, passive coatings cannot easily remove larger or heavier sand grains that dominate soiling in desert environments.

Active systems, on the other hand, try to physically detach particles from the PV surface. Among these, electrostatic cleaning has emerged as a particularly promising concept. Early implementations, such as traveling-wave electrostatic devices and oscillating field mechanisms [7], demonstrated effective particle removal without the need for water or mechanical contact. The technique holds promise for scalable, automated employment. Nevertheless, the existing work also reveals significant unresolved challenges. Firstly, the interaction between electrostatic forces and the diverse physical properties of desert sand has not been sufficiently characterized. Secondly, environmental influences, particularly humidity, substantially affect charge transfer mechanisms through the formation of thin water films on particle surfaces, yet the threshold humidity values governing this transition remain largely undetermined. Thirdly, the development of transparent conductive electrodes that maintain PV optical efficiency and also function effectively as electrostatic actuators poses a complex materials challenge. Although transparent conductive films (TCFs) such as SnO_2:F have been proposed, their relative performance, durability, and cost-effectiveness in field conditions have not been sufficiently evaluated. Finally, economic analyses of large-scale electrostatic cleaning implementations remain scarce, with few studies reconciling the trade-off between cleaning efficiency and system cost over the module lifecycle. These gaps indicate that, while electrostatic cleaning represents a promising advancement, experimental validation and economic assessment are lacking.

This leads to the research question of this study: Can a water-free electrostatic cleaning system using a transparent conductive film electrode be engineered to effectively remove diverse desert sand particles while maintaining PV module efficiency and demonstrating economic feasibility for large-scale deployment?

3. The Electrostatic Cleaning Method

3.1 Assessment of Forces Impacting Sand Particle Deposition on PV Modules

On glass surfaces, the deposition of dust particles is influenced by three forces: the adhesive force F_A, the gravitational force F_G and the electrostatic force F_E [8]. If an ideal spherical sand particle is assumed, F_A can be described using the equation [9]:

$$F_{\mathrm{A}} = \frac{Ar}{6Z_0^2} \tag{1}$$

where A is the Hamaker constant, which varies for each material, r is the particle radius and Z_0 is the separation distance between the surfaces of the electrode plate and the particle. Israelachvili's (1992) simplified version of the Lifshitz theory of van der Waals forces can be used to describe the Hamaker constant using the equation [10]:

$$A = \frac{3}{4}kT\left(\frac{\varepsilon_1-\varepsilon_3}{\varepsilon_1+\varepsilon_3}\right)\left(\frac{\varepsilon_2-\varepsilon_3}{\varepsilon_2+\varepsilon_3}\right) + \frac{3hf_e}{8\sqrt{2}}\frac{\left(n_1^2-n_3^2\right)\left(n_2^2-n_3^2\right)}{\left(n_1^2+n_3^2\right)^{1/2}\left(n_2^2+n_3^2\right)^{1/2}\left\{\left(n_1^2+n_3^2\right)^{1/2}+\left(n_2^2+n_3^2\right)^{1/2}\right\}} \tag{2}$$

It describes two bodies made of different materials interacting via a medium. The first term of the equation describes the Debye and Keesom interactions, while the second term describes London dispersion interactions. The glass of PV modules is mainly composed of noncrystalline amorphous SiO_2 [11], commonly known as silica, while desert sand is primarily made up of trigonally symmetric SiO_2 [12], commonly referred to as quartz. In practice, photovoltaic cover glass is typically toughened soda–lime glass, which contains minor amounts of Na_2O and CaO in addition to SiO_2. These additives slightly modify the permittivity ε and refractive index n, and therefore may influence the resulting electrostatic forces. However, for the purpose of theoretical estimation, the properties of pure amorphous silica ($\varepsilon_1 \approx 3.8$, $n_1 \approx 1.5$) are used as a reasonable approximation [10],[13]. Quartz has $\varepsilon_2 \approx 1.5$, $n_2 \approx 1.6$ [14], [15]. The medium between the two bodies is air with $\varepsilon_3 \approx 1$, $n_3 \approx 1$. The letter k corresponds to the Boltzmann constant and h corresponds to the Planck constant. The temperature T is assumed to be 300 K, as the permittivity values were determined at this temperature. Furthermore, 300 K is close to the IUPAC standard temperature. f_e is the electronic absorption frequency in the ultraviolet spectrum. Given the relationship of

$$f_e = \frac{c}{\lambda} \tag{3}$$

with c being the speed of light and $\lambda = 210$ nm being the wavelength used to determine the refractive index values. The absorption frequency can be estimated as $f_e \approx 1.4 \cdot 10^{15}\ \mathrm{s}^{-1}$. Using these values, Israelachvili's simplification of the Hamaker constant (Eq. (2)) yields $A \approx 4.5 \cdot 10^{-20}$ J. To calculate the adhesive force using Eq. (1), the surface separation distance Z_0 between the particle and the glass must be determined. The primary minimum, which describes the separation distance with the strongest van der Waals interaction between two surfaces, is assumed to be $Z_0 \approx 4 - 10$ Å. It commonly lies between $Z_0 \approx 4 - 10$ Å, [9].

doi: 10.7795/320.202601

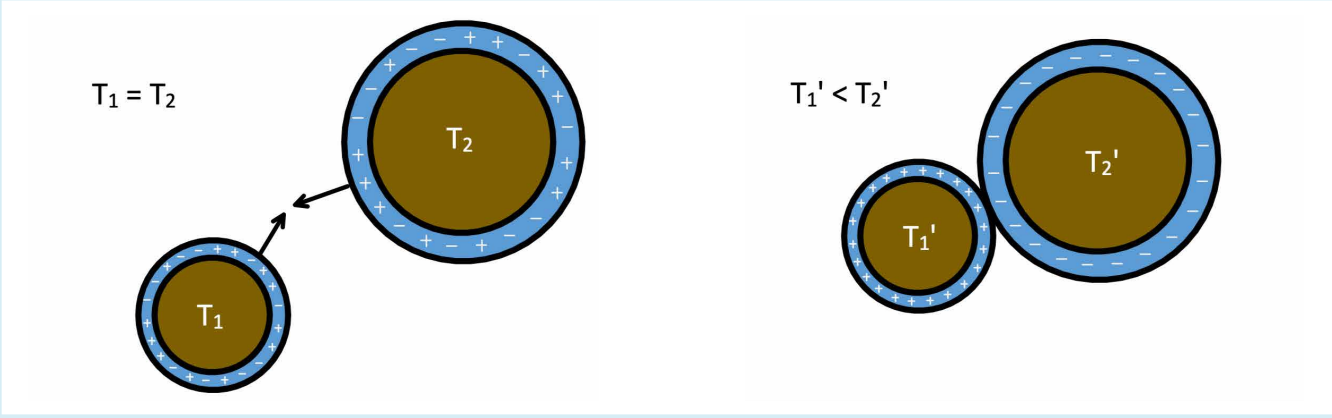

Fig. 1: Charge Acquisition of Sand Particles. The schematic depicts a collision of two differently sized particles, in which the friction force works to generate heat, resulting in a difference in temperature T. It causes the water layer of the larger particle to acquire a negative charge and the water layer of the smaller particle to acquire a positive charge.

If the same ideally spherical particle is assumed, F_G can be described using the equation

$$F_G = \frac{4}{3}\pi r^3 \rho g \tag{4}$$

where r is the particle radius, g is gravitational acceleration and ρ is the quartz density, which is approximately $\rho = 2650\ \mathrm{kg/m^3}$ [16].

PV modules are typically installed at an inclined angle to maximize solar irradiance [17]. Consequently, to determine the resultant perpendicular gravitational force $F_{G\perp}$, F_G must be multiplied by the cosine of the angle θ between the module's surface and the ground:

$$F_{G\perp} = F_G \cdot \cos(\theta) \tag{5}$$

As the angle of inclination increases, the magnitude of the perpendicular gravitational force $F_{G\perp}$ decreases.

The origin of the electrostatic force, F_E, is generally attributed to triboelectric charging, where frictional contact occurs between airborne dust particles and between the dust and the glass surface. While the precise underlying mechanisms remain a subject of active research, a detailed model has been proposed by Gu et al. (2013) [18]. In this model, F_E arises due to aerial collision of dust particles and between dust particles and glass. These collisions generate heat through frictional forces [18]. Temperature differences arise between the bodies involved due to uneven collisions. At a high enough humidity, the sand particles form a water layer on their surfaces [8]. The humidity level for which a water layer is formed will be explored in the chapter „Determining the Minimum Humidity Required for the Formation of a Water Layer".

The equilibrium reaction of water, represented by

$$H_2O_{(l)} + H_2O_{(l)} \rightleftharpoons H_3O^+(aq) + OH^-(aq) \tag{6}$$

is sensitive to temperature. According to this theory, temperature shifts alter the ion concentrations in the water layers. Citing ab initio simulations that show H_3O^+ diffuses much faster than OH^- [19], the model suggests that frequent collisions lead to an uneven ion distribution. It is proposed that particles at higher temperatures preferentially accumulate OH^- ions (yielding a negative charge), while cooler particles gather more H_3O^+ ions (leading to a positive charge), as depicted in Fig. 1. As described by Coulomb's law, this charge separation would create an attractive force between particles and the glass, significantly complicating the cleaning of PV modules [8].

Among the three forces, namely F_A, $F_{G\perp}$ and F_E the dominant force acting on a sand particle deposited on a PV module is the electrostatic force [8]. This force significantly influences the amount of sand deposition. As a result, conventional cleaning methods often prove ineffective in removing dust particles that have been deposited electrostatically [20].

3.2 The Concept of the Electrostatic Cleaning Method

To address the issue of electrostatically deposited sand particles, an electrostatic cleaning method emerges as a promising alternative. In this approach, any pre-existing electrostatic attraction force can be neglected. This is because the electrostatic cleaning method charges the surfaces of both the sand particle and the PV module, thereby removing any previous charge. Furthermore, the electrostatic cleaning method introduces an external opposite charged electrode placed above the PV module. With sufficient charge, the external electrode attracts the sand particles on the glass. It then lifts them off the surface and down the slope of the PV module, effectively removing them. The forces acting on a sand particle when using the electrostatic method are

doi: 10.7795/320.202601

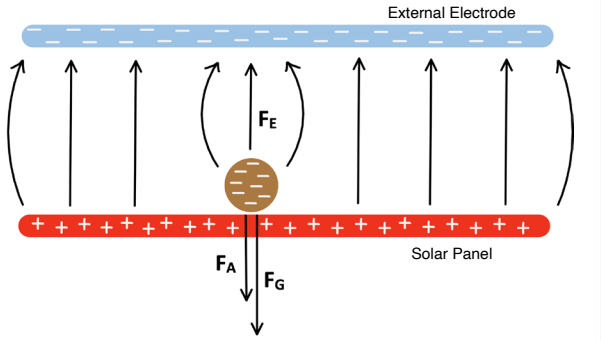

Fig. 2: Different Forces Acting on a Sand Particle. The schematic depicts a charged sand particle deposited on a PV module. It illustrates the forces exerted on the particle and their corresponding orientations. The figure includes the adhesive force F_A, the gravitational force F_G and the electrostatic force F_E.

depicted in Fig. 2.

F_E, the force lifting the particle, can be expressed using the equation for an isolated charge in an electric field:

$$F_E = E \cdot q \tag{7}$$

In this equation, E represents the applied electric field, and q denotes the electric charge of the particle. For a sphere in contact with a charged plane, the electric charge q can be estimated as follows [21]:

$$q = \frac{2}{3}\pi^3 r^2 \varepsilon E \tag{8}$$

where r denotes the radius of the sphere, ε represents the permittivity and E denotes the applied electric field, as stated earlier. The permittivity ε can be computed as the product of the electric field constant ε_0 and the permittivity $\varepsilon_1 = 4.637$ of crystalline SiO_2 [13], as shown in Eq. (9).

$$\varepsilon = \varepsilon_0 \varepsilon_1 \tag{9}$$

3.3 Determining the Required Field Strength for Particle Removal

To assess the potential limitations of the electrostatic cleaning method, an equation was formulated. This equation determines the field strength required to overcome the adhesive (F_A) and gravitational ($F_{G\perp}$) forces acting on a deposited sand particle. Since F_E acts in the opposite directions of both F_A and $F_{G\perp}$ as shown in Fig. 2, an equation can be set up, where F_E is equal to the sum of F_A and $F_{G\perp}$:

$$0 = F_E - F_A - F_{G\perp} \tag{10}$$

To be solved for the electric field E, the terms in Eq. (10) must be substituted with Eq.s (1–9). When transformed and solved for the electric field strength, the equation can be expressed as follows:

$$E = \sqrt{\frac{\frac{Ar}{6Z_0^2} + \frac{4}{3}\pi r^3 \rho g \cos(\theta)}{\frac{2}{3}\pi^3 r^2 \varepsilon_0 \varepsilon_r}} \tag{11}$$

3.4 Titanium Dioxide as Transparent Conductive Thin Film

The proposed electrostatic cleaning method achieves the removal of sand particles through the application of a potent electric field. This electric field is established by employing an electrode covering the PV module and an external electrode situated above the PV module. The external electrode can be made from various conductive materials. However, the PV module's covering electrode requires a material with both high transparency and effective electrical conductivity to avoid hindering the module's performance. Transparent Conductive Films (TCFs) play a fundamental role in modern optoelectronics and photovoltaics as these specialized materials combine outstanding optical transparency with robust electrical conductivity. While Titanium Dioxide (TiO_2) is not commonly utilized as a TCF due to its limited electrical conductivity [23], it is renowned for its exceptional optical properties and versatile applications [23]. Furthermore, TiO_2 possesses intrinsic self-cleaning properties making it an attractive material for the proposed electrostatic cleaning method. TiO_2 demonstrates photocatalytic activity when exposed to ultraviolet (UV) irradiation, resulting in the oxidation and decomposition of organic contaminants present in its immediate vicinity. The absorption of UV-rays, the generation of $OH^{\cdot}$, as well as the recombination are depicted in Reactions 12 to 18 [24].

$$TiO_2 + h\nu \rightarrow e^- + h^+_{vb} \tag{12}$$

$$h^+_{vb} \rightarrow h^+_{tr} \tag{12'}$$

$$O_2 + e^- \rightarrow O_2^{\bullet -} \tag{13}$$

$$O_2^{\bullet -} + O_2^{\bullet -} + 2H^+ \rightarrow H_2O_2 + O_2 \tag{14}$$

$$O_2^{\bullet -} + h^+_{vb} \rightarrow O_2 \tag{15}$$

$$O_2^{\bullet -} + h^+_{tr} \rightarrow O_2 \tag{15'}$$

$$OH^- + h^+_{vb} \rightarrow OH^{\bullet} \tag{16}$$

$$OH^{\bullet} + OH^{\bullet} \rightarrow H_2O_2 \tag{17}$$

$$e^- + h^+_{tr} \rightarrow \text{recombination} \tag{18}$$

doi: 10.7795/320.202601

The initial step, as shown in Reac. (12), entails the exposure of TiO_2 to ultraviolet light, triggering the onset of the photocatalytic reaction. Under the UV irradiation, TiO_2 absorbs a photon (hv), instigating the generation of an electron (e^-) in the conduction band and a valence band hole $\left(h^+_{vb}\right)$. Reac. (12') depicts the process by which these valence band holes become trapped on the TiO_2 surface, leading to the formation of trapped holes $\left(h^+_{tr}\right)$ [24]. Unlike their valence band counterparts, trapped holes exhibit no mobility within the material, rendering them incapable of oxidizing water. Reac. (16) depicts the creation of hydroxyl radicals ($OH^{\cdot}$), with Reac. (17) showing the combination of two radicals to yield hydrogen peroxide (H_2O_2). In the short interval prior to the combination of H_2O_2 (Reac. (17)) $OH^{\cdot}$ radicals can engage in oxidative interactions with closeby organic matter, starting their oxidation and decomposition. Reac.s (15), (15') and (18) depict the processes of electron recombination with the valence band and trapped holes, respectively. The distinctive photocatalytic characteristics of TiO_2 make it a promising candidate for PV module cleaning. This is primarily due to its ability to decompose and oxidize organic contaminants upon UV exposure. Furthermore, it is imperative to acknowledge that the synthesis of TiO_2 is characterized by both cost-effectiveness and, notably, its exceptional non-toxic nature [25]. These qualities collectively underscore the environmental sustainability and economic viability of TiO_2 as electrode material for electrostatic cleaning. It is important to note that in practical environments, deposition of sand and dust on PV surfaces can shield the TiO_2 layer from incident UV radiation, thereby reducing its photocatalytic effectiveness. The proposed electrostatic cleaning method can mitigate this limitation by removing particulate contamination, helping to restore exposure of the TiO_2 surface to UV light and maintain its self-cleaning functionality.

4. Experimental Methods

4.1 Measuring the Adhesive Force at Different Humidities

Silicon dioxide (SiO_2), which makes up the majority of desert sand [12], is a well-known electrical insulator [22]. For desert sand to become conductive and therefore susceptible to the electrostatic cleaning method, it needs to form a water layer on its surface. This water layer is commonly formed by absorbed water moisture [8]. Desert climates typically have low atmospheric humidity. Therefore, it is necessary to establish the minimum humidity required for a water layer to form on a particle's surface. This determination is pivotal in establishing the specific humidity range within which the proposed electrostatic cleaning method can be implemented effectively.

Thus, an experiment was set up in which the adhesive force between a 32 µm-sized sand particle and a neutralized mineral glass substrate was measured using an atomic force microscope (MFP3D, Asylum Research, Santa Barbara) equipped with a tipless probe (HQ:NSC35/TIPLESS/AL BS, Mikromasch) (see Fig. 4). The values were measured in a humidity controlled chamber at three different relative humidity levels. Control over the humidity conditions was achieved by introducing either water vapor or nitrogen gas, resulting in an increase or decrease in relative humidity, respectively. The humidity level was monitored using a thermo-hygrometer (TH-130, Hama). Measurements were not acquired for humidities above 32 % to avoid damaging the electronics of the measuring device. To ensure accurate measurements, a hygrometer was positioned close to the probe measuring the adhesive force. This placement mitigated the impact of non-uniform humidity distribution within the chamber. In total, the adhesive force was measured at 600 different locations and at three different levels of relative humidity between the two surfaces.

4.2 Particle Size Analysis

To gain deeper insights into the range of particle sizes that the electrostatic cleaning method must remove, an investigation into the possible sand sizes was conducted. Five different types of sand were analysed: marine sand (Aquariensand, Hornbach), Timbuktu sand, Inner Erg Chebbi sand, Outer Erg Chebbi sand (donated by Dr. M. Weiss), and Negev sand (donated by Dr. G. Mekler). The procedure involved spreading the sand particles uniformly on a 1 mm x 1 mm grid paper. Subsequently, the particles were magnified using a microscope (HM-Lux 3, Leitz), and detailed images were captured with a digital camera (12MP dual camera system, Apple). The subsequent phase involved a digital comparative analysis of the sand particles against the grid substrate, thereby allowing for precise determination of the sand particle sizes. A total of 700 measurements were taken, with each particle type being subjected to approximately 140 measurements. It should be noted that the optical resolution of this system is approximately 20 µm. Particles smaller than this limit could not be measured accurately and were excluded from the analysis.

For experimentally validating the theoretical charge estimations from Eq. (8), a dedicated setup was constructed. This setup consisted of two parallel, horizontal aluminium plate electrodes (30 cm x 30 cm, Torex Handels AG) separated by insulating spacers to maintain a precise distance of 6 mm. The process was recorded using high-speed videography. For each measurement the following procedure was performed:

Particle Placement: A single sand particle, with a pre-measured radius, was placed onto the center of the lower electrode.

Recording: The high-speed camera was activated to record the gap between the electrodes. The experiment was then

doi: 10.7795/320.202601

started by applying a 6 kV potential from a high-voltage power supply (SF power supply 6 kV, Awyco AG) across the electrodes, generating an electric field of 1 MV/m.

Particle Motion: The electric field induced a charge on the particle and exerted an upward electrostatic force. This force overcame gravity, causing the particle to lift off the bottom electrode and accelerate towards the top electrode.

Data Extraction: The high-speed video footage was analysed frame-by-frame to measure the particle's total time of flight (t). This was measured as the time interval between the first frame showing particle liftoff and the frame showing contact with the upper electrode.

This time measurement was then used to deduce the particle's charge (q) through the logic outlined in Eq.s (7-9). First, the particle's mass (m) was calculated from its known size and density.

$$m = \frac{4}{3}\pi r^3 D \tag{19}$$

m denotes the mass of the particle and D corresponds to its density.

Second, using the measured time (t) and knowing the travel distance (x), the particle's net upward acceleration was determined, and the total upward force was calculated, accounting for the counteracting force of gravity.

$$a = \frac{2x}{t^2} + g \tag{20}$$

a denotes acceleration, x represents the separation distance between two electrodes, t signifies the time elapsed and g stands for gravitational acceleration.

Finally, from this force and the known electric field strength (E), the charge (q) was deduced.

$$q = \frac{ma}{E} \tag{21}$$

q signifies the electric charge of the particle, m is the mass and E denotes the strength of the electric field.

This procedure was repeated for 120 measurements across ten different particles with sizes ranging from 460 to 1170 µm. The measurements were conducted within a humidity range of 40 to 45 %. Smaller sizes were excluded due to resolution limitations of the videography equipment.

4.3 Production of Transparent Conductive Thin Film

For the synthesis of a TiO_2 thin film, a sol-gel method was employed [26], [27]. Initially, a precursor solution was prepared by dissolving titanium tetra-isopropoxide (TTIP, 98 %+, VWR) in isopropanol (98 %+, VWR) at a concentration of 0.1 M. Specifically, 1.4 g of TTIP were diluted with isopropanol to achieve a final volume of 50 ml. The resulting solution was carefully mixed in a Pyrex beaker through manual stirring with a glass rod for a duration of 10 minutes, all under ambient conditions. In parallel, a mineral glass substrate measuring 15 mm x 10 mm (Mineralglas, Jumbo) underwent cleaning with ethanol and acetone. For the coating process, an improvised Mayer rod was crafted. The construction of the Mayer rod entailed tightly winding a steel thread (Kupferrohr Biegefeder, Rothenberger Industrial) with a diameter of 1.2 mm around an aluminum rod. A Mayer rod with a 0.6 mm thread size yields an approximate dry film thickness of 4 µm. This assumes a coating with approximately 6 % solids by volume [28]. Each coating cycle comprised the deposition of 3 ml of the prepared precursor solution onto one edge of the glass substrate. Subsequently, the Mayer rod was positioned upon the solution and uniformly drawn across the surface of the substrate at an approximate speed of 10 cm/s. Following this, the substrate was dried at room temperature for 25 minutes. The entire procedure was repeated for varying numbers of cycles to yield films with different thicknesses. Upon the conclusion of the coating cycles, the coated substrate underwent an annealing process within a muffle furnace (LT 5/14, Nabertherm), where it was annealed at a temperature of 450 °C for 6 hours and left to cool down for 2 hours. This annealing procedure induced structural transformations within the coated film, encompassing three distinctive phases. The initial phase entailed hydrolysis, as depicted by Reac. (22). Subsequently, the process advanced to the initial condensation stage, wherein a single water molecule was split-off. This chemical transformation is portrayed in Reac. (23). Ultimately, the second condensation stage led to the separation of three water molecules, culminating in the formation of a thin crystalline titanium dioxide film that adhered to the substrate. This reaction progression is symbolized by Reac. (24).

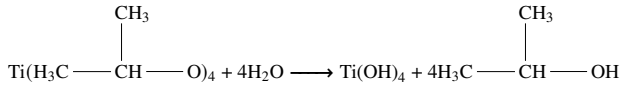

(22)

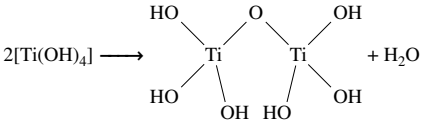

(23)

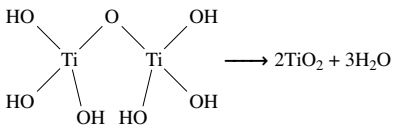

(24)

The procedure was repeated seven times for varying numbers of cycles. The films were magnified under a microscope and ultimately digitally analysed. It is noted that only the anatase phase of TiO_2 exhibits strong photocatalytic activity. While the annealing procedure at 450 °C is commonly reported to favour the formation of anatase, the precise crystal phase of the films in this study was not directly characterized.

4.4 Determining the Efficiency of an Electrostatic Cleaning Prototype

In order to assess the effectiveness of the proposed electrostatic cleaning method, an experiment was conducted to evaluate its capability to remove marine sand (Aquariensand, Hornbach) from the electrodes under different conditions. The measurements were performed at surface inclinations of 5°, 10°, and 20°, with three different electrodes and under different electric field strengths. The first electrode was a 30 cm x 30 cm aluminium sheet (Torex Handels AG) with the specific intention of establishing a reference point for the subsequent measurements involving transparent electrodes. The second electrode was a 30 cm x 30 cm glass substrate (Mineralglas, Jumbo) coated with four cycles of TiO_2 and the third electrode was a 30 cm x 30 cm x 0.3 cm glass substrate coated with a fluorine doped tin oxide (SnO_2:F) thin film (TCO30-8, Solaronix).

To ensure a clear and repeatable procedure, the manual cleaning process was systematized. The handheld apparatus consisted of a 30 cm long, 3 cm wide aluminium bar electrode (Torex Handels AG), fitted with non-conductive spacers at each end to ensure a consistent 6 mm separation from the surface electrode. The experimental protocol was as follows:

Sand Deposition: Initially, 5 g of marine sand were uniformly deposited onto the surface of the electrode under investigation.

System Energization: The stationary plate electrode was connected to a positive potential, and the handheld bar electrode was connected to a negative potential (SF power supply 6 kV, Awyco AG). The voltage was varied for different measurements, with a maximum of 6 kV.

Cleaning: A cleaning cycle was defined as the complete cleaning of the entire electrode surface. To perform one cycle, the operator started at a top corner of the plate electrode. The bar electrode was moved downward in a single, continuous sweep at a constant velocity of approximately 5 cm/s. Upon reaching the bottom, the wand was lifted, moved horizontally to an adjacent, slightly overlapping position, and another downward sweep was performed. This sequence of overlapping downward sweeps was repeated until the entire surface of the 30 cm x 30 cm electrode had been covered. As sand was lifted by the wand, it was carried downward and fell off the bottom edge of the plate. The entire cleaning process for a single measurement consisted of performing three such complete cycles.

Measurement of Remaining Sand: Following the three cleaning cycles, any sand remaining on the plate electrode was carefully collected, and its mass was recorded.

4.5 Determining the Energy Requirement of the Electrostatic Cleaning Method

In order to assess the feasibility and practicality of the proposed electrostatic cleaning method, it is essential to determine the total energy requirement associated with it. The total energy required to clean the PV module surface using the proposed method can be expressed by the following equation:

$$E_{\text{total}} = E_{\text{charging}} + E_{\text{removal}} \tag{25}$$

Within this equation, E_{charging} represents the energy essential for the charging of the two cleaning electrodes, while E_{removal} denotes the energy dissipated during the removal of sand particles. The energy stored in the capacitor formed by the electrodes, E_{charging}, can be calculated using the equation [29], [30]:

$$E_{\text{charging}} = \frac{\varepsilon S}{2d} U^2 \tag{26}$$

Here, ε characterizes the permittivity of air, and S designates the surface area of the handheld cleaning electrode. E_{charging} exhibits a direct proportionality to the square of the applied voltage (U^2) and an inverse proportionality to the separation distance of the electrodes (d). In contrast, determining the energy required for the removal of contaminants, denoted as E_{removal}, is more complex. The formulation for E_{removal} is shown in Eq. (27) as a series summation [31], [32]:

$$E_{\text{removal}} = 2\pi\varepsilon r U^2 k \sum_{n=0}^{\infty} c_n \tag{27}$$

In this context, r signifies the radius of the sand particles, while k represents the number of total sand charging cycles of all the sand particles, defined by the ensuing expression:

$$k = m\frac{4}{3}\pi^3\rho N \tag{28}$$

Within this equation, m stands for the mass of the sand deposited on the PV module, ρ denotes the sand's density, and N is an estimate of the average number of charging and discharging cycles each sand particle experiences until removal. Additionally, c_n is the coefficient, as defined by the subsequent expression:

$$c_n = \frac{2\sqrt{\xi\,(2+\xi)}}{e^{(1+2n)\operatorname{acosh}(1+\xi)} - 1} \tag{29}$$

doi: 10.7795/320.202601

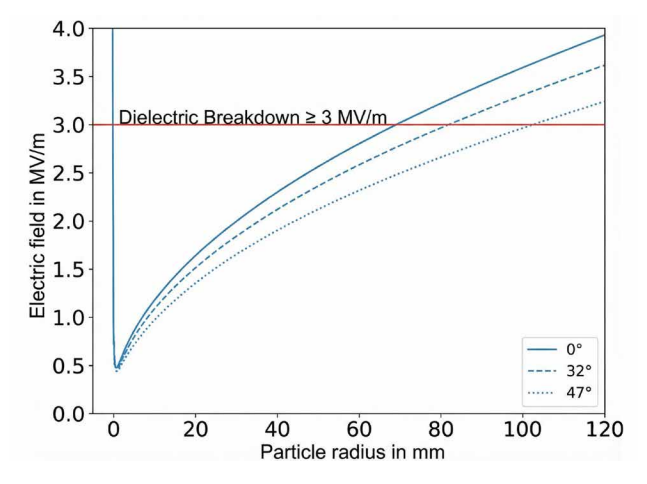

a) Large Particle Radius Scale

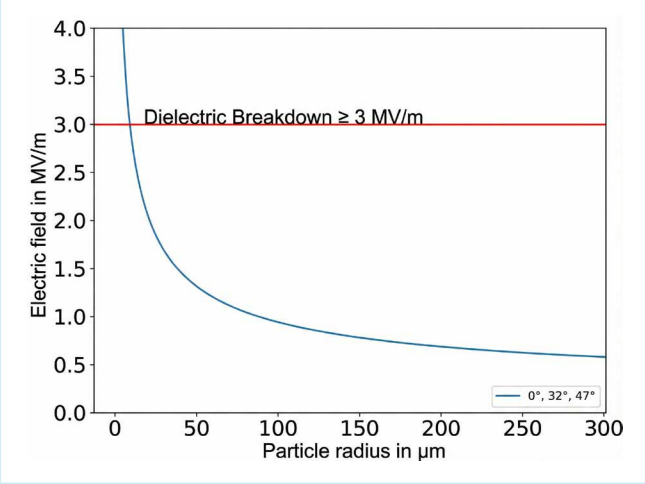

b) Small Particle Radius Scale

Fig. 3: Required Field Strength for Particle Removal. The electric field strength required to remove sand at different particle sizes calculated using Eq. (11). The values were determined for three different PV module inclinations (equator: 0°, upper Sahara: ~ 32°, central Europe: ~ 47°). Particle sizes requiring a field strength of $E \geq 3$ MV/m are impossible to remove using the proposed electrostatic method.

where $\xi = d/r$ characterizes the parameter that elucidates the spacing relative to the size of the spherical particles. An estimate for the value of $\sum_{n=0}^{\infty} c_n$ can be determined numerically. Using the experimental parameters of $d = 6$ mm (derived from an electric field of 1 MV/m at 6 kV) and a mean particle radius of $r = 168$ µm, yields the parameter $\xi \approx 35.7$. Due to the exponential term in the denominator, the series converges extremely rapidly. For all practical purposes, the infinite sum can be approximated, yielding $\sum_{n=0}^{\infty} c_n \approx 1.014$. The surface area S of the cleaning electrode is taken to be 90 cm^2.

4.6 Determining PV Module Efficiency when Utilizing Transparent Conductive Films

Despite the high transmittance properties exhibited by Transparent Conductive Films (TCFs), TCFs still exhibit absorption and reflection characteristics. To quantify the extent of power loss attributable to these characteristics, measurements were conducted using three different materials. In this study, two 0.5 W PV modules (Solarmodul 0.5 W, 70 mm x 55 mm x 3 mm, 8.2V, Seeed Studio) were used, one served as a control and remained uncovered, while the other was covered with one of the three different cover materials. The cover materials included a 3 mm thick glass substrate with no coating, a substrate with a SnO_2:F coating and a substrate with four cycles of TiO_2 coatings. Voltage and current measurements were recorded simultaneously from the covered and the uncovered module and subsequently compared. A total of 105 measurements were taken (35 for each material).

5. Results and Discussion

5.1 Minimal Field Strength Required for Particle Removal

Fig. 3 was set up using the values from Eq. (11). The figure depicts the necessary field strength to mitigate F_A and F_G for sand particles of all sizes. Although air is an excellent insulator, it breaks down at field strengths greater than $E \geq 3$ MV/m. At this point, it becomes conductive and causes the electric field between the electrodes to discharge [33]. The theoretical operational range for this electrostatic method on a non-inclined PV module is limited to particles with radii between 10 µm and 7 cm. In the case of smaller particle sizes, large F_G dominates. Both F_G and F_A ultimately cause the required field strength to fall within the range of dielectric breakdown. A related study by Panat and Varanasi (2022) found the electrostatic effect to be constrained to particles with a radius of $r \geq 32$ µm and $r \leq 9$ mm [34]. The cause for these differing results is that F_E was calculated using a different estimation of the acquired particle charge q, where this study estimates q to be approximately 1.65 times larger.

5.2 Evaluation of a Water layer Formation Threshold

Fig. 4 depicts the measured F_A-values of the 32 µm-sized sand particle and the mineral glass substrate. The estimated F_A using Eq. 1 of a 32 µm-sized particle is 698 nN. It is observed that most measurements in Fig. 4 at humidity levels of 13 % and 23 % fall below the estimated value, exhibiting mean values of 302 nN and 557 nN, respectively. This discrepancy from the estimated value may be attributed to a reduced contact

doi: 10.7795/320.202601

area resulting from surface roughness. A previous study found a similar result, with F_A being greatly reduced due to a smaller contact area [34]. Conversely, when exposed to a relative humidity of 32 %, the measured F_A in Fig. 4 exhibits a mean value of 4297 nN, which significantly surpasses the estimated value of 698 nN. This sharp increase is attributed to the formation of a capillary bridge between the hydrophilic surfaces of the particle and the glass substrate. At this humidity level, the resulting capillary attraction becomes the dominant component of the adhesion force [35], [36]. The data therefore implies the existence of a critical humidity threshold between 23 % and 32 % for the formation of this liquid bridge, which is essential for the proposed cleaning method.

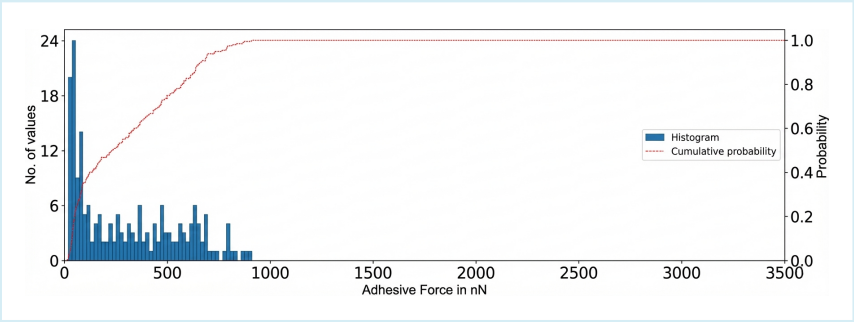

a) Humidity 13 %

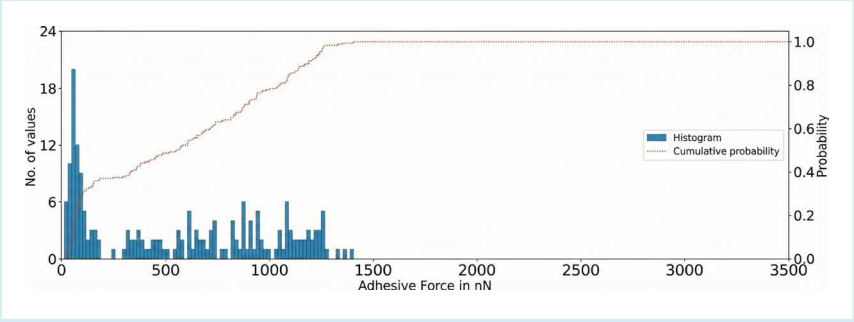

b) Humidity 23 %

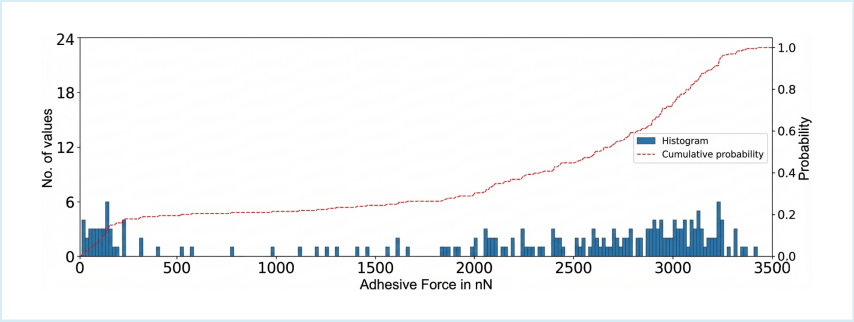

c) Humidity 32 %

Fig. 4: Histogram of the AFM Measurements. The adhesive force between a 32 µm sand particle and a glass surface was measured at 600 different locations and under three different relative humidity levels using a MFP3D atomic force microscope. Humidity levels were controlled using nitrogen gas and water vapor. Measurements with humidities above 32 % were not acquired. Prior to the measurements, the glass surface was electrostatically neutralized using a deionizer to eliminate residual charge.

5.3 Assessment of Sand Particle Sizes

Fig. 5 illustrates an analysis of various sand types conducted through digital imaging. The sand samples under investigation encompassed marine sand, Timbuktu sand, Inner Erg Chebbi sand, Outer Erg Chebbi sand, and Negev sand, which exhibited mean particle sizes of 336 µm, 277 µm, 285 µm, 246 µm, and 130 µm, respectively. While the definition of sand can vary based on the classification system used, engineers and geologists typically characterize sand as particles falling within the diameter range of 20 m to 2 mm [12], which agrees with the measured values. The digital microscopy system used had an effective optical resolution of approximately 20 µm due to image contrast and grid calibration (see Fig. 6). Consequently, particles smaller than this threshold could not be resolved with sufficient accuracy and were therefore excluded from the analysis.

This limitation explains the low representation of sub-50 µm particles in most samples. It is acknowledged that airborne contaminants responsible for PV surface soiling are typically finer, sometimes below 10 µm. The present measurements were thus intended to represent the upper end of particle sizes that can adhere to module surfaces in desert environments and to evaluate electrostatic cleaning effectiveness under such conditions. A more detailed analysis of sub-10 µm dust particles is recommended for future work. It is noteworthy that all measured particles of the various sand types investigated in this study do not extend into the dielectric breakdown range illustrated in Fig. 3. This suggests that, under the tested conditions, the proposed electrostatic cleaning approach is capable of effectively removing larger sand particles from PV module surfaces, while finer dust particles (< 10 µm) may require further examination.

5.4 Evaluation of Charge Measurements

Fig. 7 depicts the experimentally measured charge values of particles (q) in contact with a 6 kV charged metal electrode

doi: 10.7795/320.202601

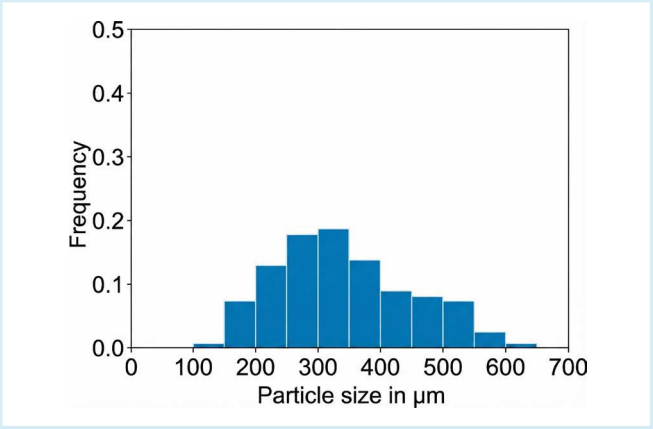

a) Marine sand

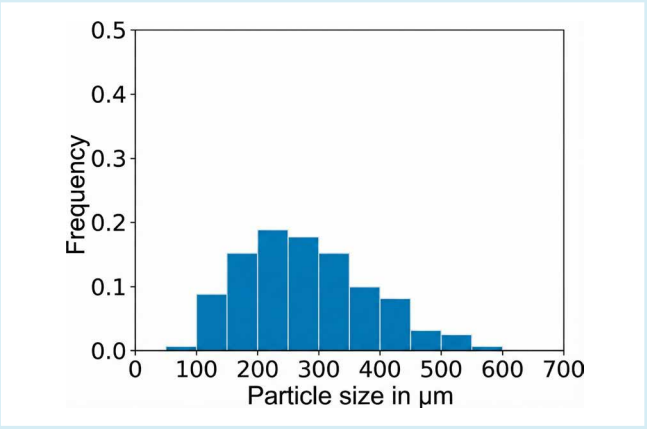

b) Timbuktu sand

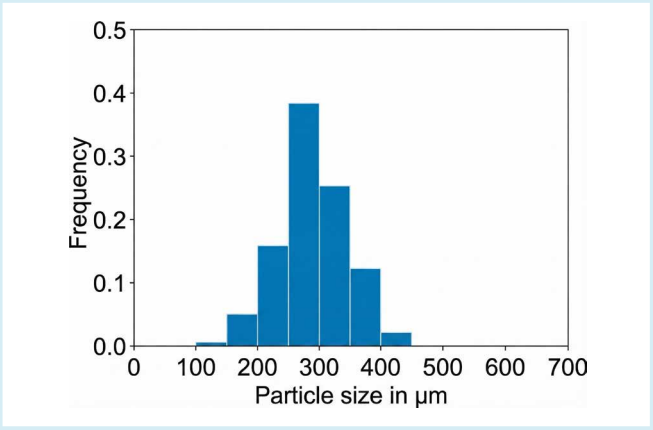

c) Inner Erg Chebbi sand

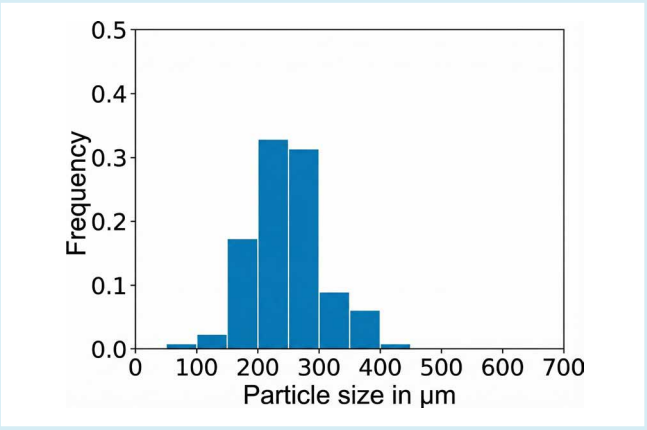

d) Outer Erg Chebbi sand

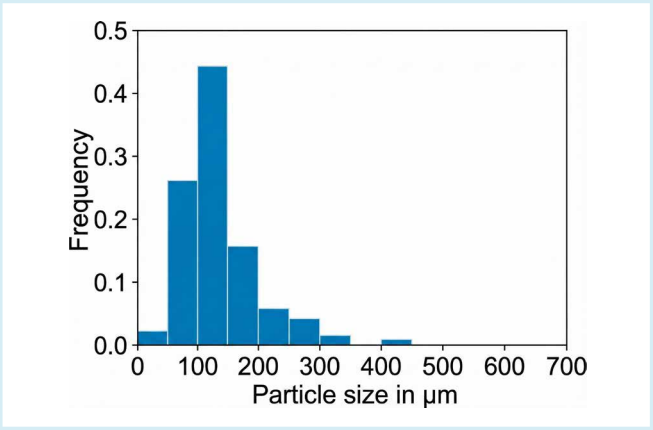

e) Negev sand

Fig. 5: Sand Particle Size Analysis. The particle size analysis of five distinct particle types was performed manually. Using a microscope, digital images of the particles were captured against a 1 mm x 1 mm grid paper background as shown in Fig. 6. Particle sizes were then determined by direct visual comparison to the grid scale in these images. A total of 700 measurements were taken, with each particle type being subjected to approximately 140 measurements.

and under the influence of a 1 MV/m strong electric field. Additionally, it depicts the estimated values for q calculated using Eq. (8) as well the estimated values by a similar study by Panat and Varanasi in 2022 [34]. The measured charge values for smaller particles align more closely with Panat and Varanasi's estimations. In contrast, the values for larger particles show better congruence with the estimations from this study.

5.5 Assessment of TiO_2 Thin Film Synthesis

As illustrated in Fig. 8, glass substrates were coated with TiO_2 using the sol-gel method. A varying numbers of coating cycles were used. Different numbers of coating cycles led to distinct TiO_2 thin film outcomes. The motivation for this was to identify an optimal thickness that balances complete surface coverage with high structural integrity.

One to two coating cycles: Surfaces A and B in Fig. 8 exhibit a discontinuous film, characterized by insufficient film

doi: 10.7795/320.202601

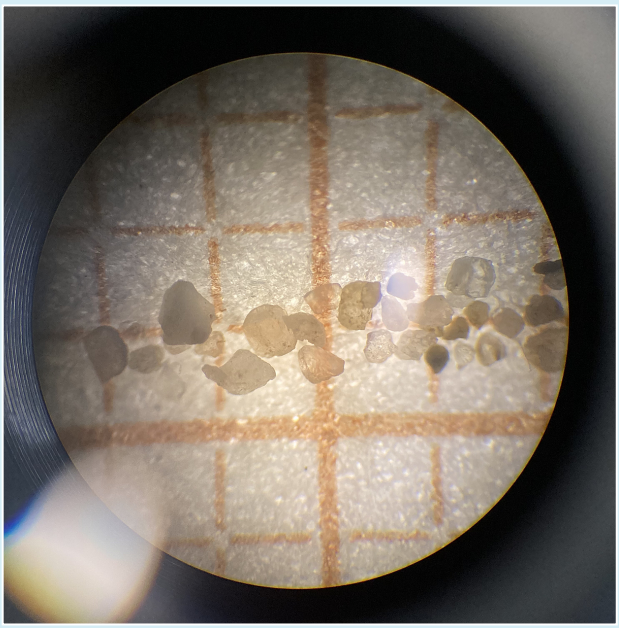

Fig. 6: Digital micrograph of marine sand particles dispersed on a 1 mm x 1mm reference grid for size characterization.

thickness, which prevented proper film formation.

Three to six coating cycles: Surfaces C, D, E, and F in Fig. 8 display continuous and well-formed films. These surfaces exhibit desirable film characteristics.

Seven coating cycles: Surface G in Fig. 8 shows a discontinuous film possibly due to the excessive deposition of the TiO_2 precursor. This excess could have hindered the completion of Reac. (22 -24), preventing the coated solution from achieving full crystallization.

Surfaces A, B and C, exhibited the presence of non-crystalline aggregates, potentially attributable to the accumulation of impurities within the film structure. Notably, a 2016 study by Chen et al. found that four to eleven coating cycles produced continuous films. In contrast, using one to three or 12 to 15 cycles resulted in films with a discontinuous or compromised structure [26]. In their investigative approach, they employed the spin coating method, maintaining a rotation speed of 2000 revolutions per minute. This method yielded notably thinner films, offering a plausible rationale for Chen et al.'s discovery of favourable film characteristics when employing higher coating cycle counts. A full characterization of the film's electrical properties, such as conductivity and resistance as a function of thickness, would provide valuable insight into its performance. However, these measurements were outside the scope of this investigation. This is a recommended direction for future studies.

5.6 Evaluation of Electrostatic Cleaning Method Efficiency

To assess the efficiency of the proposed electrostatic cleaning method, measurements were performed under various conditions and surface inclinations. The measured values are illustrated in Fig. 9. These evaluations were conducted using three distinct types of electrodes. Measurements involving the aluminum electrode served as a reference for the subsequent two assessments carried out with the transparent electrodes. The aluminium electrode has a high electrical conductivity of approximately $3.5 \cdot 10^7$ S/m [37]. When subjected to a 1 MV/m electric field, it cleared all sand within three cleaning cycles at inclinations of 10° and 20°.

Conversely, the SnO_2:F electrode under identical conditions, with an electrical conductivity of approximately 41.7 S/m [38], demonstrated notable sand removal, albeit not as effectively as the aluminum electrode. Similarly, the TiO_2 electrode, operating under identical conditions and exhibiting a significantly lower electrical conductivity in the range between 0.1 and 10^{-6} S/m [37], exhibited satisfactory sand removal capabilities, achieving clearance of approximately half of the deposited sand. These results depict effective sand removal capabilities of both SnO_2:F and TiO_2 electrodes.

The significant difference in cleaning efficiency can be attributed to the role of electrical conductivity in maintaining a uniform surface charge density. The high conductivity of the aluminium electrode allows for the rapid transport and

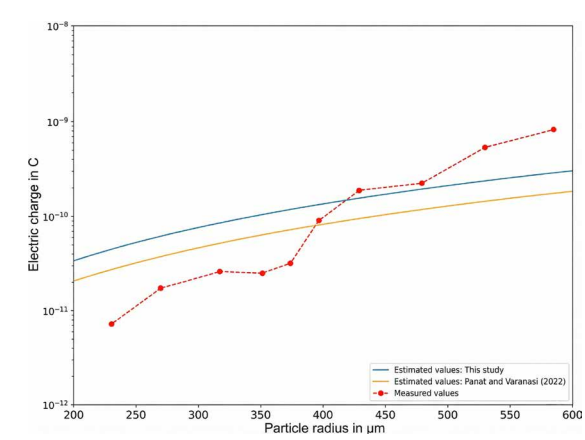

Fig. 7: Experimental Charge Measurements. A total of 120 measurements were conducted on 10 particles with sizes ranging from 460 to 1170 µm. Each particle underwent 12 velocity assessments, and the corresponding electric charge values were determined utilizing Eq.s 19 to 21. The figure illustrates the measured values, the previously estimated values calculated using Eq. 8 and the estimated values by Panat and Varanasi [34].

doi: 10.7795/320.202601

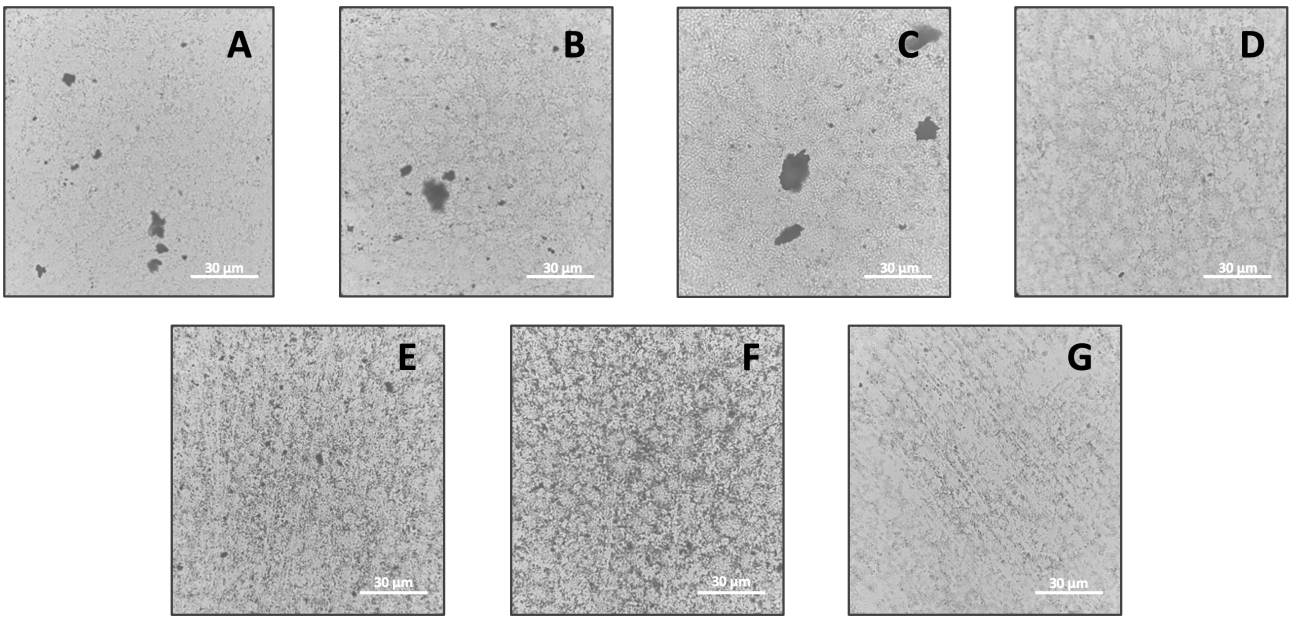

Fig. 8: Magnified Surface of TiO_2 Thin Film with Varying Thickness. A ≈ 4 µm (1 cycle), B ≈ 8 µm (2 cycles), C ≈12 µm (3 cycles), D ≈16 µm (4 cycles), E ≈ 20 µm (5 cycles), F ≈ 24 µm (6 cycles), G ≈ 28 µm (7 cycles)

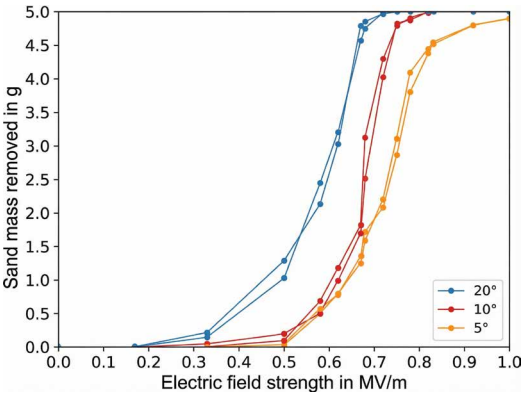

a) Aluminium Electrode

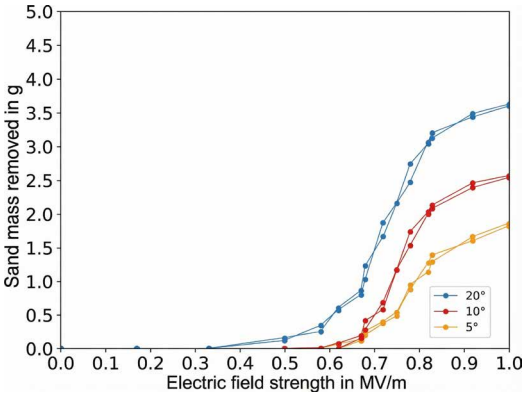

b) Titanium Dioxide Electrode

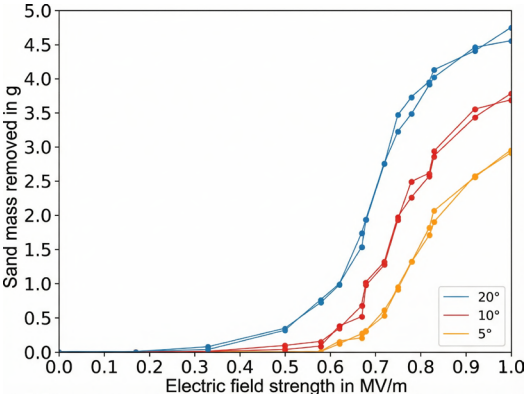

c) Fluorine Doped Tin Oxide Electrode

Fig. 9: Electrostatic Cleaning Efficiency under Different Conditions. A comprehensive evaluation encompassing a total of 180 measurements was executed across three distinct electrodes, employing 5 g of marine sand as the test medium. Each electrode underwent assessments at surface inclinations of 5°, 10°, and 20°. These measurements were conducted under 15 different electric field strengths, with each specific measurement protocol repeated twice to ensure data consistency.

doi: 10.7795/320.202601

replenishment of charge across its surface. When a sand particle is charged and lifted, the local charge on the surface is depleted. On the aluminium electrode, this charge is almost instantaneously replenished by the flow of electrons from adjacent areas, maintaining a consistently strong and uniform electric field required for effective particle removal. In contrast, the low conductivity of the TiO_2 electrode impedes this charge transport. This leads to localized charge depletion on the surface, creating areas with a temporarily weaker electric field that is insufficient to overcome the adhesion forces of nearby particles. The SnO_2:F electrode, with its intermediate conductivity, represents a compromise between these two extremes, resulting in moderate cleaning efficiency.

This raises the question of how much the remaining sand reduces electricity production. While power output of partially cleaned modules was not directly measured, an estimate can be made based on the experimental data. In the case of the TiO_2 electrode at a 20° inclination and 1 MV/m field strength, approximately 1.5 g of the initial 5 g of sand remained (Fig. 9). The initial soiling density on the 30 cm x 30 cm (0.09 m^2) surface was 55.6 g/m^2, representing severe test conditions. The remaining 1.5 g corresponds to a residual soiling density of approximately 16.7 g/m^2. Assuming a conservative linear power loss of 1.7 % per g/m^2 of soiling [40], this residual sand would cause an estimated power loss of approximately 28 %. Therefore, under these severe conditions, the cleaning process restored the module to approximately 72 % power generation. The total power output would also be affected by the inherent power loss of the TCF itself. For the TiO_2 coated module, this would result in a combined power reduction of approximately 58 % (29.7 % from the film). This shows the trade-off between the material properties and the overall energy generation performance.

Considering these findings, it becomes relevant to examine their implications for real-world deployment. Notably, many of the world's major desert regions are located in the Northern Hemisphere, spanning latitudes between the 20th and 40th northern latitudes [41]. PV modules are commonly aligned with latitudinal inclinations to maximize solar irradiance [17]. This practice suggests our proposed cleaning method is highly promising for practical implementation, particularly at inclinations above 20°. In a comparative context, an earlier investigation conducted by Kawamoto in 2018 employed parallel screen electrodes for electrostatic sand removal [42]. Kawamoto's study involved cleaning efficiency measurements on a larger 100 cm x 100 cm surface inclined at 30° initially loaded with 10 g/m^2 of sand. In harmony with the findings of this study, Kawamoto (2018) reported favourable cleaning rates when using voltages of 6 kV and higher. Nevertheless, it is worth emphasizing that the present study involved measurements with a higher initial sand deposition of 56 g/m^2 on a smaller 30 cm x 30 cm surface and at lower inclinations of 5°, 10°, and 20°. Compared directly with Kawamoto's findings,

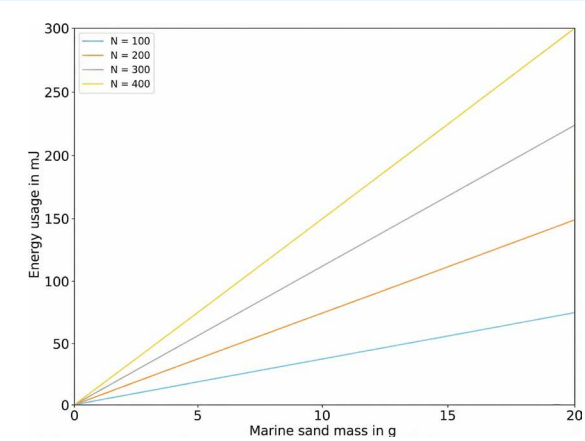

Fig. 10: Energy Requirement of Electrostatic Cleaning. This figure illustrates the energy requirement evaluation for the electrostatic cleaning method, computed using Eq.s (25-29). The analysis assumes a 1 MV/m electric field for sand cleaning. The variable *N* represents the average number of charging and discharging cycles per sand particle, with estimations intentionally set conservatively higher.

the electrostatic cleaning method in this study demonstrates significantly enhanced dust cleaning capabilities.

5.7 Assessment of Energy Requirement

Eq.s (25–29) were used to determine the energy requirement of the proposed electrostatic cleaning method. As depicted in Fig. 10, it is evident that the energy consumption remains remarkably low, even when confronted with significant quantities of deposited sand. With a known dust accumulation rate of approximately 0.3 g/m^2 per day in regions such as North Africa and the Middle East [43], the proposed electrostatic cleaning method is able to remove a year's worth of sand deposition, equivalent to approximately 110 g/m^2, while requiring a mere 1.5 J/m^2 of electrical work. This finding holds considerable promise for the practical implementation, as the energy costs for the cleaning operation itself are negligible.

5.8 PV Module Efficiency using Transparent Conductive Films

Transparent Conductive Films (TCFs) seem an obvious choice as electrode materials to cover PV modules, due to their high conductivity and transmittance. However, it is important to acknowledge that TCFs still possess absorption and reflection characteristics, which results in decreased PV module efficiency and subsequent power loss. To quantify the power loss associated with the application of TCFs on PV modules, a series of measurements was conducted. Subsequent analysis of the recorded measurements revealed mean power losses of 7.3 %, 20.6 %, and 29.7 % for PV modules covered with a plain

doi: 10.7795/320.202601

glass substrate, a SnO_2:F coated substrate, and a TiO_2 coated substrate, respectively. The power loss of the SnO_2:F coated substrate and the TiO_2 coated substrate were substantial although expected. TiO_2 coated substrates typically show transmittance values of 75-90 % [26]. The SnO_2:F coated substrate's manufacturer stated a minimum transmittance of 65 %. A power loss of 29.7 % and 20.6 % indicate an actual transmittance of approximately 70.3 % and 79.4 % respectively, which is in line with the expected values. These findings reveal a key challenge in applying electrostatic cleaning techniques. Continued research is needed to refine the balance between cleaning effectiveness and power generation, as well as to enhance TCF transmittance.

5.9 Maintenance Cost and Economic Benefit

In regions with arid climates, maintaining the efficiency of solar panels poses a significant challenge. The conventional method of removing contamination from PV modules involves expensive water-based cleaning techniques. To quantify this cost, the following equation can be formulated:

$$R_{\text{loss}} = C \cdot T + \frac{D_{\text{eff}} \cdot R_{\text{total}}}{2T} \tag{30}$$

Here, R_{loss} and R_{total} denote the revenue lost and the total potential revenue, respectively, both measured in \$/day. C denotes the cost of a single cleaning instance in \$, T signifies the cleaning rate measured in units of 1/day and D_{eff} indicates the efficiency decay rate of the solar module in %/day. According to Faes et al.'s measurements in 2019, the average relative performance loss (D_{eff}) is reported to be 0.21 % [44]. Assuming a washing cost (C) of approximately 1300 \$/MW [45], and an electricity price of approximately 60 \$/MWh, Eq. (30) yields maintenance costs of about 100 \$/day when cleaning the 1 MW solar modules at 15-day intervals.

Calculating the cost implications of adopting the electrostatic cleaning method proposed in this study, it is necessary to account for both the installation expenses and later maintenance costs. As determined in „Determining the Energy Requirement of the Electrostatic Cleaning Method", the energy consumption for the electrostatic process itself is negligible. The practical electricity costs are therefore dominated by the operational method: The cleaning process can be accomplished either automatically using cleaning robots or by employing cleaning personnel. Specifically, the increase in electricity costs for the automatic cleaning system amounts to approximately 60 cent per cleaning session. This is predicated upon a power consumption of 150 W and an operational duration of roughly 60 hours, considering a cleaning rate of 0.05 m^2/s and three cleaning cycles [46]. It further assumes a total solar module surface area of approximately 6000 m^2, with each individual solar module occupying an area of 2 m^2 [47].

Alternatively, manual cleaning of a 1 MW installation by personnel likewise necessitates approximately 60 hours of labor. To clarify this manual procedure and address how the critical electrode separation distance is maintained, the process envisions a trained operator using a scaled-up version of the handheld cleaning wand used in the experiments. This tool would consist of a long aluminium electrode bar, wide enough to cover a significant portion of a solar module in a single pass. Crucially, non-conductive, low-friction polymer guides or rollers would be mounted at the ends of the wand. These guides would rest on and slide along the frame of the PV module, ensuring a constant separation distance is maintained between the electrode and the module's glass surface without direct contact or scratching. The operator's task would be to systematically sweep this wand down the face of each module. The electrostatic force performs the actual cleaning, so the required physical effort is minimal and any time needed to stop and clean the electrode is eliminated. This process forms the basis for the estimated 60 hours of labour. At an hourly wage of 12 \$, this equals 900 \$ per cleaning session, yielding maintenance costs of about 60 \$/day when cleaning solar modules at 15 day intervals [45], [48].

Electrostatic cleaning, whether manual or automatic, significantly reduces maintenance costs for solar modules. Manual cleaning yields a 40 % reduction of the 1300 \$/MW washing cost. This equates to approximately 440,000 \$ or 190 \$/module saved over the 30-year lifespan of the solar module installation. Meanwhile, automatic cleaning offers a 99.5 % maintenance cost reduction. This totals at around 1,240,000 \$ or 550 \$/module over the same period. These cost reductions amount to roughly 5 % and 14 % of the total potential revenue generated, respectively. Therefore, if the installation expenses are lower than the saved maintenance costs, the electrostatic cleaning method demonstrates economic viability.

With a 1 MW installation, the solar panel's total surface area is roughly 6000 m^2, with individual modules each spanning 2 m^2 [47]. Using fluorine-doped tin oxide coated glass as the surface electrode, the material cost estimate stands at approximately 72,000 \$ assuming a conservative rate of 12 \$/ m^2 [49]. Despite the potential for further reduction in material costs through the utilization of titanium dioxide-coated glass, current constraints in industrial production render the use of titanium dioxide infeasible. Incorporating the automatic cleaning setup introduces additional material expenses. Each cleaning robot, designed to cover three modules, costs approximately 1,700 \$, totalling 1,300,000 \$ for a 1 MW installation [46]. These material costs overshadow the potential savings in maintenance expenses, even without factoring in transportation and installation costs. In contrast, the manual cleaning setup allows for roughly 160 \$/module for installation and transportation expenses over lifespan. It

doi: 10.7795/320.202601

Tab.1: Breakdown of operational costs, savings, and economic viability for water-based, manual, and automatic cleaning systems.

	Water-Based	Manual	Automatic
Cleaning Cost ($/MW)	1,300	900	~ 0.60
Maintenance Cost ($/day)	100	60	< 1
Cost Reduction (%)	Baseline	40	99.5
Total Savings ($)	Baseline	440,000	1,240,000
Savings/Module ($)	Baseline	190	550
Revenue Saved (%)	Baseline	5	14
Material Cost ($)	Baseline	72,000	1,300,000
Economic Viability	Standard	Potentially Viable	Currently Infeasible

is anticipated that installation and transportation costs will fall below 160 $/module, thereby affirming the economic advantage of the manual electrostatic cleaning method.

However, it is important to note that this economic analysis focuses on operational savings and does not account for the permanent revenue loss resulting from the TCF's reduced light transmittance, as determined in Section 4.8. A complete economic assessment would require offsetting the calculated savings with this loss. Therefore, the practical viability of this method is contingent on future advancements in highly transparent conductive films. A comparable study conducted by Faes et al. has demonstrated savings of approximately 25 $/module by employing an electrodynamic cleaning method [44]. It is likely that this study's cost estimation will coincide with Faes et al.'s calculations after installation and transportation expenses are subtracted. These findings demonstrate the potential economic viability of the manual electrostatic cleaning method but also underscore the necessity for further research in optimizing automatic cleaning systems.

5.10 Practical Implementation and Safety Considerations

A critical aspect for the practical deployment of this technology is ensuring the safety of personnel and wildlife from the high voltages involved. The 6 kV potential used in this study necessitates robust safety measures to prevent accidental contact with the electrodes. The implementation of these measures would differ between the manual and automatic cleaning approaches. For a manual system, safety would rely on a combination of equipment design and operator protocol. The handheld electrode must be designed with a fully insulated, non-conductive handle. It must also have non-conductive polymer guides at its ends to ensure a constant electrode gap. Finally, a system needs to be in place, which de-energizes the electrode immediately if released. Operators would be required to wear appropriate personal protective equipment (PPE), including high-voltage insulating gloves and footwear, and receive specific training on safe operational procedures [50].

For an automatic system, the primary safety strategy would involve isolating the solar array. This would be achieved through standard measures for high-voltage installations, such as perimeter fencing and prominent warning signage indicating the electrical hazard. The system should be designed to operate autonomously, preferably during times with minimal human or animal activity.

Crucially, for both systems, the power supply must be current-limited. By designing the power source to deliver a maximum current well below the lethal threshold (e.g., in the low milliampere range), the risk of serious injury can be drastically mitigated even in the event of accidental contact [51]. Integrating these standard electrical safety protocols is essential for transitioning the proposed cleaning method from a laboratory prototype to a commercially viable and safe technology.

6. Conclusion

This paper examined a novel approach to address the pressing issue of sand contamination of PV modules in desert regions. The accumulation of micro-particles on PV modules has posed a significant challenge to the efficient operation of photovoltaic power systems, particularly in arid areas. Existing cleaning methods are often costly, environmentally harmful, and not effective in removing electrostatically deposited dust particles. This study's research introduced an electrostatic cleaning method that offers a sustainable, cost-effective, and waterless solution to this pressing environmental and economic problem.

The paper determined the required field strength for particle removal, evaluated the minimum humidity necessary for water layer formation on sand particles, analysed the range of sand particle sizes that the proposed method can effectively remove, and measured the charges of particles under the influence of electric fields. Additionally, the research

doi: 10.7795/320.202601

explores the synthesis of Transparent Conductive Films as an ideal material for covering PV modules, with a focus on the environmental sustainability and economic viability of Titanium Dioxide (TiO_2) as an electrode material.

Experimental results demonstrated the effectiveness of the electrostatic cleaning prototype under various conditions and surface inclinations, highlighting its potential for practical implementation in desert environments. Moreover, the energy consumption analysis showed minimal energy usage, making it a feasible choice for module cleaning. However, the application of Transparent Conductive Films, while beneficial for cleaning purposes, does introduce power loss due to absorption and reflection characteristics. This challenge underscores the need for ongoing research to optimize the balance between cleaning efficiency and power generation in PV modules.

Lastly, the study calculated the economic benefit of utilizing the electrostatic cleaning method, considering both the manual and automatic cleaning approach. The findings indicate the economic feasibility of the manual cleaning approach, whereas the automatic cleaning approach did not demonstrate comparable economic viability.

In summary, the research successfully demonstrates that a water-free electrostatic cleaning system using a transparent conductive film electrode can be engineered to effectively remove diverse desert sand particles while largely maintaining PV module efficiency and demonstrating economic feasibility for large-scale deployment via a manual activation method. This offers a promising solution to a significant problem in renewable energy. It has the potential to improve the cost-effectiveness and sustainability of photovoltaic power generation in desert regions.

Acknowledgements

I would like to express my sincere gratitude to Dr. Waldemar Feller and Roger Scharpf, my project supervisors, for their guidance and continuous support throughout this research. I am deeply thankful to Simon Scherrer and ETH Zürich for providing laboratory space, AFM equipment, and invaluable assistance. I also wish to thank Dr. Martin Weiss and Dr. Gabrielle Mekler for generously providing sand samples for this project. Special thanks go to Martin Lussi for his help in acquiring materials and arranging laboratory access. I am especially grateful to Professor Franz Baumgartner, my Schweizer Jugend Forscht juror, for his great expertise and encouragement. Finally, I thank Dr. Adrien Cornaz and Dr. Mark Heinz for their insights, invaluable support, and their commitment to inspire and foster scientific curiosity among young researchers like me.

References

[1] Duggal, H. Interactive: How much of your country's electricity is renewable? 2023; https://www.aljazeera.com/amp/news/2022/1/20/interactive-how-much-of-your-countrys-electricity-is-renewable-infographic.
[2] Adinoyi, M. J.; Said, S. A. Effect of dust accumulation on the power outputs of solar photovoltaic modules. Renewable Energy 2013, 60, 633–636.
[3] Pearce, F. In Scramble for Clean Energy, Europe Is Turning to North Africa. 2023; https://e360.yale.edu/features/africa-europe-solar-wind-power.
[4] pv Europe Cleaning in the desert: A race against the sand. 2019; https://www.pveurope.eu/planning/cleaning-desert-race-against-sand.
[5] Humood, M.; Beheshti, A.; Polycarpou, A. A. Surface reliability of annealed and tempered solar protective glasses:Indentation and scratch behavior. Solar Energy 2017, 142, 13–25.
[6] Sayyah, A.; Horenstein, M. N.; Mazumder, M. K. Energy yield loss caused by dust deposition on photovoltaic panels. Solar Energy 2014, 107, 576–604.
[7] Kawamoto, H.; Shibata, T. Electrostatic cleaning system for removal of sand from solar panels. Journal of Electro-statics 2015, 73, 65–70.
[8] Liu, X.; Yue, S.; Li, J.; Lu, L. Study of a dust deposition mechanism dominated by electrostatic force on a solarphotovoltaic module. Science of The Total Environment 2021, 754, 142241.
[9] Ranade, M. B. Adhesion and Removal of Fine Particles on Surfaces. Aerosol Science and Technology 1987, 7,161–176.
[10] Israelachvili, J. N. Intermolecular & Surface Forces, 2nd ed.; Academic Press, 1992.
[11] of Encyclopædia Britannica, T. E. glass — Definition, Composition, & Facts; Encyclopædia Britannica, Inc., 2022.
[12] of Encyclopædia Britannica, T. E. Sand — Beach, Dune, & Desert; Encyclopædia Britannica, Inc., 2022.
[13] Fontanella, J.; Andeen, C.; Schuele, D. Low-frequency dielectric constants of α-quartz, sapphire, MgF2, and MgO. Journal of Applied Physics 1974, 45, 2852–2854.
[14] Malitson, I. H. Interspecimen Comparison of the Refractive Index of Fused Silica*,†. Journal of the Optical Society of America 1965, 55, 1205.
[15] Ghosh, G. Dispersion-equation coefficients for the refractive index and birefringence of calcite and quartz crystals. Optics Communications 1999, 163, 95–102.
[16] Bridges, S.; Robinson, L. Drilled solids calculations. A Practical Handbook for Drilling Fluids Processing 2020, 105–137.
[17] McCabe, L. What's the Best Direction and Angle for My Solar Panels? 2022; https://www.energysage.com/solar/solar-panel-performance-orientation-angle/.
[18] Gu, Z.; Wei, W.; Su, J.-W.; Yu, C. W. The role of water content in triboelectric charging of wind-blown sand. Scientific Reports 2013, 3.
[19] Chen, M.; Zheng, L.; Santra, B.; Ko, H.-Y.; DiStasio Jr, R. A.; Klein, M. L.; Car, R.; Wu, X. Hydroxide diffuses slower than hydronium in water because its solvated structure inhibits correlated proton transfer. Nature Chemistry 2018, 10, 413–419.
[20] Mittal, K. L.; Jaiswal, R. Particle Adhesion and Removal; John Wiley & Sons, 2015.
[21] Bishop, K. J. M.; Drews, A. M.; Cartier, C. A.; Pandey, S.; Dou, Y. Contact Charge Electrophoresis: Fundamentals and Microfluidic Applications. American Chemical Society 2018, 34, 6315–6327.

doi: 10.7795/320.202601

[22] Group, H. Q. Quartz Glass Products — Quartz Properties. 2022; https://www.heliosquartz.com/prodotti/proprieta-del-quarzo/?
[23] Patra, D. Titanium dioxide — Description & Uses; Encyclopædia Britannica, Inc., 2023.
[24] Hirakawa, T.; Nosaka, Y. Properties of O 2 • - and OH • Formed in TiO 2 Aqueous Suspensions by Photocatalytic Reaction and the Influence of H 2 O 2 and Some Ions. American Chemical Society 2002, 18, 3247–3254.
[25] V¨olz, H. G. et al. Pigments, Inorganic. Ullmann's Encyclopedia of Industrial Chemistry 2006,
[26] Chen, W.-F.; Koshy, P.; Sorrell, C. C. Effects of film topology and contamination as a function of thickness on the photo-induced hydrophilicity of transparent TiO2 thin films deposited on glass substrates by spin coating. Journal of Materials Science 2015, 51, 2465–2480.
[27] Marien, C. B. D.; Marchal, C.; Koch, A.; Robert, D.; Drogui, P. Sol-gel synthesis of TiO2 nanoparticles: effect of Pluronic P123 on particle's morphology and photocatalytic degradation of paraquat. Environmental Science and Pollution Research 2016, 24, 12582–12588.
[28] Buschman Estimate Wet Film Thickness based on Thread Size. 2020; https://buschman.com/resources/calculators/thread-size-to-wet-film-thickness/.
[29] OpenStax 19.5 Capacitors and Dielectrics; College Physics; OpenStax, 2016.
[30] of Tennessee Knoxville, U. Capacitor. 2019; http://labman.phys.utk.edu/phys222core/modules/m2/capacitors.html.
[31] Crowley, J. Simple Expressions for Force and Capacitance for a Conductive Sphere near a Conductive Wall. 2008.
[32] Maxwell, J. C. A Treatise on Electricity and Magnetism; Cambridge University Press, 2010.
[33] Tipler, P. A. Physics; Worth Publishers, 1976.
[34] Panat, S.; Varanasi, K. K. Electrostatic dust removal using adsorbed moisture–assisted charge induction for sustainable operation of solar panels. Science Advances 2022, 8.
[35] Mahdi, F.-T.; Michael, K.; Hans-J¨urgen, B. Influence of Humidity on Adhesion: An Atomic Force Microscope Study. Journal of Adhesion Science and Technology 2008, 22, 181–203.
[36] Butt, H.; M., K. Surface and Interfacial Forces; Wiley, 2018.
[37] for Nondestructive Evaluation, I. S. U. C. Nondestructive Evaluation Techniques : Eddy Current Testing. 2023; https://www.nde-ed.org/NDETechniques/EddyCurrent/ET_Tables/ET_matlprop_Aluminum.xhtml.
[38] Solaronix TCO30-8 - Conductive Glass Substrates - Electrode Materials - Solaronix Online Shop. 2023; https://shop.solaronix.com/electrode-materials/conductive-glass-substrates/tco30-8.html.
[39] Earle, M. D. The Electrical Conductivity of Titanium Dioxide. Physical Review 1942, 61, 56–62.
[40] Said, S. Z.; Islam, S. Z.; Radzi, N. H.; Wekesa, C. W.; Altimania, M.; Uddin, J. Dust impact on solar PV performance: A critical review of optimal cleaning techniques for yield enhancement across varied environmental conditions. Energy Reports 2024, 12, 1121–1141.
[41] Martin, M. Michael Martin - Wissen - Planet W¨uste - W¨usten der Nordhalbkugel - Einf¨uhrung. 2024; https://www.michael-martin.de/de/wissen_planet_wueste/wuesten_der_nordhalbkugel.html.
[42] Kawamoto, H. Electrostatic cleaning equipment for dust removal from soiled solar panels. Journal of Electrostatics 2019, 98, 11–16.
[43] Guo, B.; Javed, W.; Figgis, B. W.; Mirza, T. Effect of dust and weather conditions on photovoltaic performance in Doha, Qatar. 2015 First Workshop on Smart Grid and Renewable Energy (SGRE) 2015,
[44] Faes, A.; Petri, D.; Champliaud, J.; Geissb¨uhler, J.; Badel, N.; Levrat, J.; Roustom, B.; Hessler-Wyser, A.; Wyrsch, N.; Ballif, C.; Getaz, G.-O.; McKarris, G.; Despeisse, M. Field test and electrode optimization of electrodynamic cleaning systems for solar panels. Progress in Photovoltaics: Research and Applications 2019, 27, 1020–1033.
[45] Shah, A. H.; Hassan, A.; Laghari, M. S.; Alraeesi, A. The Influence of Cleaning Frequency of Photovoltaic Modules on Power Losses in the Desert Climate. Sustainability 2020, 12, 9750.
[46] Technology, M. E. Best MULR1650-3 G Automatic Solar Panel Cleaning Robot for Length 1650mm*3 Solar Panel Manufacturer and Factory — Multifit. 2024; https://www.vmaxpowerpv.com/solar-panel-cleaning-robot-product/.
[47] Solar, A. About 1 MW Solar Power Plant Specifications & Price in India (2023). 2023; https://amplussolar.com/blogs/1mw-solar-power-plant.
[48] Institute, E. R. Cleaner Salary in Morocco. 2024; https://www.erieri.com/salary/job/cleaner/morocco.
[49] KGaA, M. Fluorine Doped Tin Oxide. 2024; https://www.sigmaaldrich.com/search/fluorine-doped-tin-oxide?focus=products&page=1&perpage=30&sort=relevance&term=Fluorine%20doped%20tin%20oxide&type=product.
[50] Occupational Safety and Health Administration Solar Energy: Electrical. 2025; https://www.osha.gov/green-jobs/solar/electrical.
[51] Purser, M. The Need for Current-Limiting Devices for Electrical Safety. 2025; https://www.oshaeducationcenter.com/overcurrent-protection.

doi: 10.7795/320.202601

doi: 10.7795/320.202601

Als Schüler*in wissenschaftlich publizieren

Wie auch aus deiner Wettbewerbsarbeit eine zitierfähige Veröffentlichung wird

Hast du Fragen? In den FAQs auf der Seite „Für Autor*innen“ findest du Antworten.

www.junge-wissenschaft.ptb.de/fuer-autorinnen

Was ist eine wissenschaftliche Veröffentlichung?

Wissenschaftliche Publikationen, sogenannte Papers, sind ein zentrales Element wissenschaftlichen Arbeitens. In Papers werden nicht nur Zeitpunkt und Stand einer Erkenntnis öffentlich dokumentiert, sondern auch mit der Wissenschafts-Community geteilt. So lässt man Kolleg*innen derselben Fachrichtung an Ergebnissen teilhaben oder zeigt progressive Forschungsansätze auf.

Was kostet die Veröffentlichung?

Für die Autor*innen fallen keinerlei Veröffentlichungsgebühren (*page charges*) an. Alle Kosten z. B. für Redaktion, Lektorat, Layout, Website und App tragen Verlag und Sponsoren. Verlag ist die Physikalisch-Technische Bundesanstalt PTB, die das Projekt seit Gründung begleitet.

Was ist besonders an einer wissenschaftlichen Veröffentlichung?

Die Besonderheit eines echten, wissenschaftlichen Papers ist, dass es *peer reviewed* ist. Der Begriff setzt sich zusammen aus den englischen Wörtern *peer* für „Kolleg*in“ und *reviewed* für „überprüft“ (*review* = die Überprüfung). Die Arbeit wird also von einem / einer meist anonymen Fachkolleg*in, der oder dem *referee*, auf Schlüssigkeit überprüft. Die Arbeit ist somit gecheckt und kann als Basis für weitere Forschungsvorhaben genutzt werden.

Wieso wissenschaftlich publizieren?

Diese Papers dienen nicht nur dem fachlichen Austausch, sondern auch als Nachweis der erbrachten Leistungen im jeweiligen Spezialgebiet. Wie ein Lebenslauf informiert die Veröffentlichungsliste über den beruflichen Werdegang und wissenschaftlichen Erfolg.

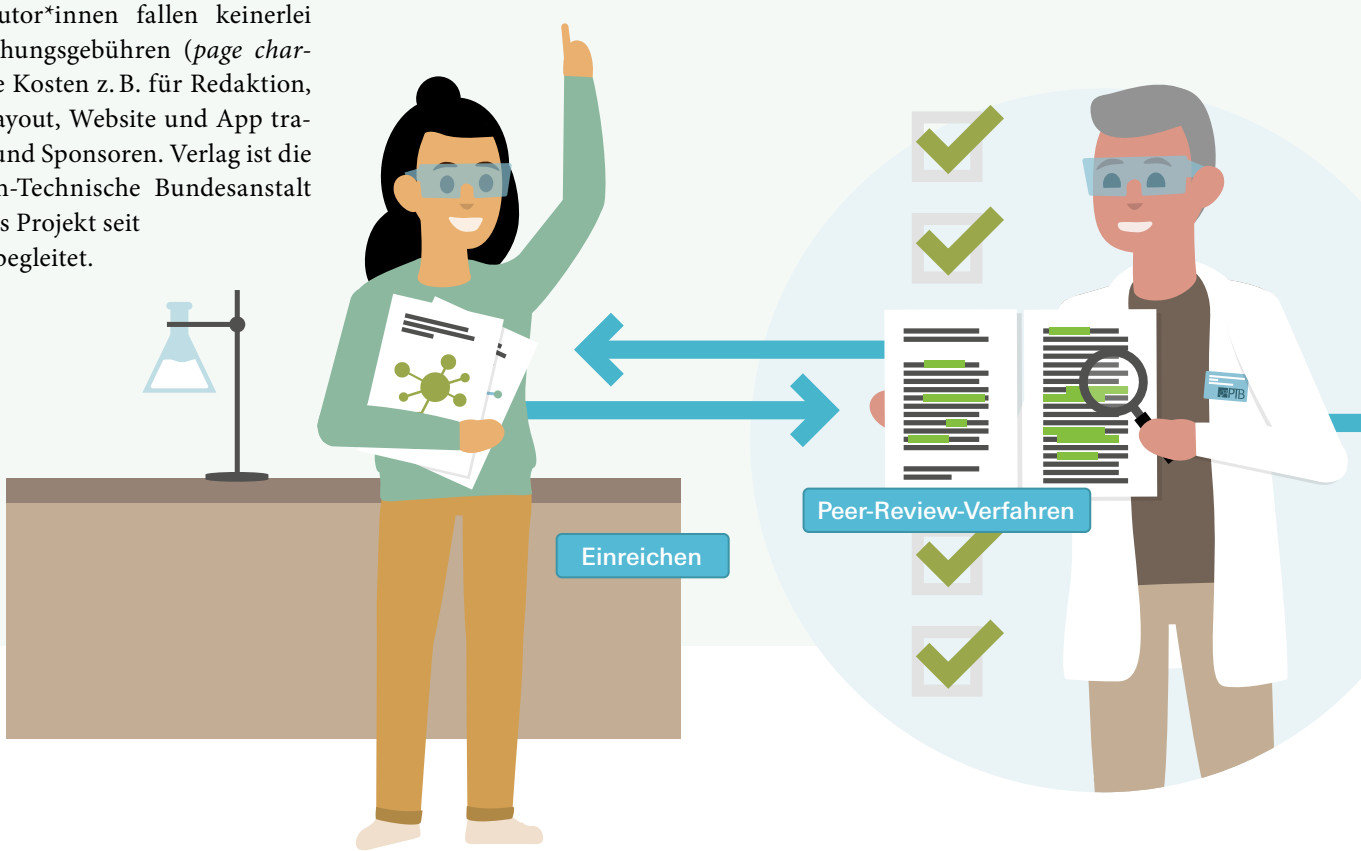

Wie geht das und wie viel Arbeit muss ich investieren?

Die Junge Wissenschaft (JuWi) ist die einzige Plattform, auf der bereits Schüler*innen ein erstes Paper, *peer reviewed*, veröffentlichen können. Das von der JuWi-Chefredaktion eingeleitete und begleitete Peer-Review-Verfahren macht aus deinem Wettbewerbsbeitrag eine zitierfähige Veröffentlichung. Ein JuWi-Paper ist der Startschuss für deine persönliche Veröffentlichungsliste. Und als erfolgreiche Teilnehmer*in eines Forschungswettbewerbs hast du den Löwenanteil der Arbeit bereits erledigt.

Sende deine Arbeit und die Erstveröffentlichungserklärung an:

Chefredaktion
Junge Wissenschaft

Dr.-Ing. Sabine Walter
Paul-Ducros-Straße 7
30952 Ronnenberg

Tel: 05109 / 561508
Mail: sabine.walter@verlag-jungewissenschaft.de

Wie geht es nach dem Einreichen weiter?

Die Chefredakteurin sucht einen geeigneten Fachgutachter*in, der bzw. die, die inhaltliche Richtigkeit der eingereichten Arbeit überprüft und eine Empfehlung ausspricht, ob sie veröffentlicht werden kann (Peer-Review-Verfahren). Das Gutachten wird dir zugeschickt und du erhältst die Möglichkeit, Hinweise des oder der Fachgutachter*in oder eigene Änderungen einzuarbeiten. Die Erfahrung zeigt, dass Arbeiten, die z. B. im Rahmen eines Wettbewerbs wie Jugend forscht die Endrunde erreicht haben, die besten Chancen haben, dieses Peer-Review-Verfahren zu bestehen. Bis hierhin hast du keinerlei Arbeit investiert.

Schließlich kommt die Arbeit in die Redaktion, wird für das Layout vorbereitet und und nach der Freigabe als Open-Access-Beitrag, also für jedermann zugänglich, veröffentlicht.

Was bringt es mir?

JuWi-Autor*innen erwerben in der engen Zusammenarbeit mit der Redaktion Kenntnis über den Aufbau einer wissenschaftlichen Arbeit, über wissenschaftlichen Schreibstil, worauf zu achten ist und welche Schritte wann notwendig sind. Autor*innen eines JuWi-Papers haben so sehr früh einen bedeutenden Teil wissenschaftlichen Publizierens erlernt, noch bevor sie an die Hochschule gehen.

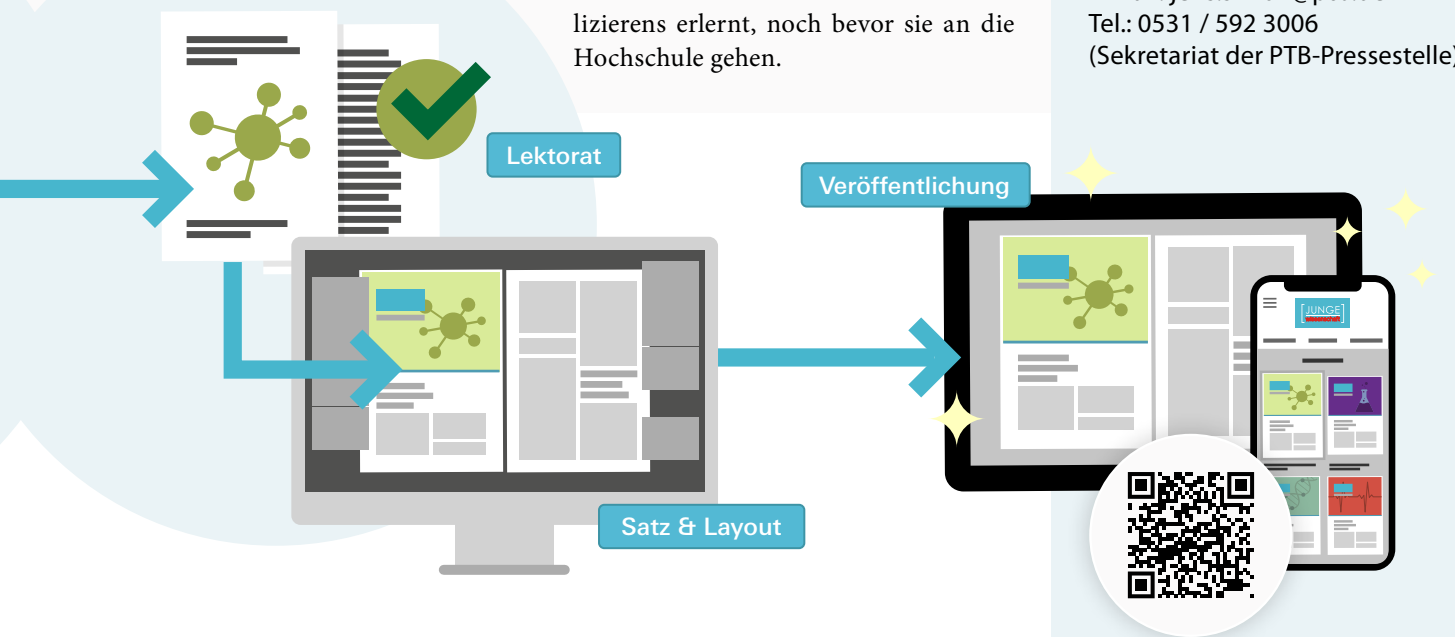

Impressum

Junge Wissenschaft
c/o Physikalisch-Technische Bundesanstalt (PTB)
www.junge-wissenschaft.ptb.de

Redaktion
Dr.-Ing. Sabine Walter,
Chefredaktion Junge Wissenschaft
Paul-Ducros-Str. 7
30952 Ronnenberg
E-Mail: sabine.walter@verlag-jungewissenschaft.de
Tel.: 05109 / 561 508

Sabine Siems, Verlag
E-Mail: sabine.siems@ptb.de
Tel.: 0531 / 592 8202

Design & Satz
Sebastian Baumeister
Art Director / stilsicher.design
E-Mail: baumeister@stilsicher.design
Tel.: 05142 / 302 99 04

Verlag
Dr. Dr. Jens Simon,
Pressesprecher der PTB
Bundesallee 100
38116 Braunschweig
E-Mail: jens.simon@ptb.de
Tel.: 0531 / 592 3006
(Sekretariat der PTB-Pressestelle)

Dein Ticket zur Wissenschaft

Jungforscher*innen publizieren
online | *peer reviewed* | original

Fahrkarte
zum sofortigen Reiseantritt
JuWi
Für:
1 Jungforscher*in
Nach:
wissenschaftlich publizieren
Über:
peer reviewed
PTB
Preis:
Gratis

Die PTB ist jetzt auch bei Instagram. Auf dem Kanal @ptb.bund findest du auch unsere JuWi-Beiträge.